

# A Study in Zucker: Insights on Human-Robot Interactions

Alex Day and Ioannis Karamouzas

**Abstract**—In recent years there has been a large focus on how robots can operate in human populated environments. In this paper, we focus on interactions between humans and small indoor robots and introduce a new human-robot interaction (HRI) dataset. The analysis of the recorded experiments shows that anticipatory and non-reactive robot controllers impose similar constraints to humans’ safety and efficiency. Additionally, we found that current state-of-the-art models for human trajectory prediction can adequately extend to indoor HRI settings. Finally, we show that humans respond differently in shared and homogeneous environments when collisions are imminent, since interacting with small differential drives can only cause a finite level of social discomfort as compared to human-human interactions. The dataset used in this analysis is available at: <https://github.com/AlexanderDavid/ZuckerDataset>.

**Index Terms**—Human-robot interaction, social robot navigation, human-aware motion planning

## I. INTRODUCTION

Given the advancements in robotics and AI in recent years along with the significant decrease in hardware cost, robots are increasingly becoming a part of our lives, from vacuuming our floors and delivering items in automated warehouses to transporting passengers autonomously in urban areas [1]. From robot vacuums to robo-taxis, studying how humans react to such robots and interact in a shared environment plays a crucial role in the further development of autonomous systems. In this paper, we focus on small service robots like Roombas that operate in indoor spaces and have to interact intelligently with humans to avoid collisions while completing their tasks. In this field, there has been a lot of recent work on *social robot navigation* aiming to steer robots in human-populated spaces [2]. Despite such efforts, existing approaches are typically evaluated from a robot-centric perspective. While the robot’s performance is important to assess the quality of employed navigation algorithms, the efficiency and safety of the humans are equally important in shared interaction settings. Unfortunately, in such settings, there is limited knowledge about how humans interact and behave in the presence of robots and, subsequently, about the *human-centered* behavior of robots. To this end, in this paper we seek to answer the following questions:

$Q_1$ : Are reactive robot controllers more effective than non-reactive ones in ensuring human safety and efficiency?

$Q_2$ : How well do state-of-the-art approaches for human trajectory prediction scale to indoor interaction settings involving humans and small differential drive robots?

$Q_3$ : Does the human-human interaction law extend to interactions between humans and indoor service robots?

We conducted a 3-day user study in the Zucker Family Graduate Education Center in Charleston, SC, USA, to address these questions. Following a brief overview of highly relevant work, we focus on the specific questions and elaborate on the related results. We hope that our findings and the collected HRI trajectories, which we share with the community, can improve human-centered service robotics, facilitating better human trajectory prediction and socially-aware robot control.

## II. RELATED WORK

### A. Human-Robot Interaction Datasets

A lot of recent work has been focusing on capturing and analyzing HRI data to better understand how humans interact with robots. The related datasets can be classified based on if the interactions they contain are unstructured or structured. Unstructured interactions can closely approximate true-to-life behavior, but require laborious manual labeling due to the lack of control in the experimental conditions. For example, Zhimon et al. [3] provide a dataset of humans interacting with an autonomous floor scrubber robot in commercial environments. The recent JRDB [4] and SCAND [5] datasets capture multimodal sensor data from a teleoperated robot interacting in indoor and outdoor environments on a university campus. In contrast to these unstructured settings, structured interactions occur in a controlled environment, typically equipped with sophisticated motion capture solutions that facilitate high-fidelity data collection and analysis. The THÖR dataset [6] is one such example capturing diverse indoor interactions between humans and between humans and a non-reactive small industrial robot following a predetermined path. The HRI datasets in [7] and [8] study the impact a robot has on humans during a crossing-gate and a corridor-exit experiment, respectively, with [7] showing that participants behave more conservatively in the presence of a robotic wheelchair than a humanoid robot. Overall, structured interactions offer high repeatability and confidence in the tracked trajectories and related results. However, they can become prohibitively expensive to set up and run, especially at a large scale. Our work releases a new structured HRI dataset containing multiple scenarios and robot controllers while lowering the barriers for conducting accurate experiments in shared indoor environments through a custom-

This work was supported by the NSF under Grant No. IIS-2047632.

The authors are with the School of Computing at Clemson University, SC, USA. {aday, ioannis}@clemson.edu. Ioannis Karamouzas is also with the University of California, Riverside, USA. ioannis@cs.ucr.edu.

made tracking system (see the supplementary material for comparisons with prior datasets).

### B. Social Robot Navigation Methods

There has been a lot of highly relevant work for autonomous and collision-free navigation of a robot amidst a crowd of humans [2]. Existing techniques for human-aware robot navigation can be broadly classified into geometric planning approaches and learning-based methods. State-of-the-art geometric planners rely on the concepts of velocity obstacles (VO) and time to collision [9], [10], and can provide formal guarantees of the collision-free behavior of robots while supporting a wide range of robot models and behaviors [11], [12]. However, they often require careful parameter tuning to achieve desired navigation results, with VO-based controllers also exhibiting overly conservative behavior as they tend to throw away too many admissible velocities to guarantee safe navigation [2]. Learning-based methods can provide more flexibility, with recent contributions taking advantage of deep reinforcement learning to enable end-to-end steering and train crowd-aware navigation policies [13]–[15]. Despite the success stories of geometric and learning-based approaches the robots do not always exhibit the level of sophistication that humans do in similar interaction scenarios. As such, researchers have been focusing on improving the control policy of a robot by accounting for interactions between all agents in the scene, expert demonstrations, social norms, human collaboration, and group-aware planning among others [16]–[22]. In this paper, we are interested in assessing the performance of three representative robot navigation algorithms in indoor physical settings. While existing works in benchmarking social robot navigation methods typically employ a robot-centric evaluation paradigm [23]–[25], here we focus on the *human-centered* performance of the interaction system by evaluating the impact that the controlled robots have on the efficiency and safety of the humans.

### C. Human Trajectory Prediction

The need for accurate methods to predict the future movements of humans based on historical observations is crucial to developing better robot simulation and navigation algorithms. To perform pedestrian trajectory prediction, early work has adopted model-based solutions that leverage hand-tuned mathematical models to encapsulate the humans’ behavior. These include models based on social forces, velocity-obstacles, and data-driven formulations [9], [10], [26], [27]. In recent years, model-based methods have been replaced by model-free approaches that rely on deep learning architectures to achieve state-of-the-art (SOTA) prediction performance. Such architectures include RNN structures for generating sequential predictions, social attention and pooling mechanisms for capturing the neighbors’ influence, and GAN architectures and conditional VAE (CVAE) models for accounting for the uncertainty and multimodality of human decision making [28]–[32]. We refer to the excellent survey of Rudenko et al. [33] for more details. Our paper considers two CVAE approaches that have shown to achieve SOTA performance in human-human



Fig. 1. (left) A still from the overhead webcam during an experimental trial. (right) Our tracking solution includes Vive Trackers 2018 attached to hats, a Vive Controller mounted on a Turtlebot, and Vive Base Stations 2.0.

interaction settings and evaluates their applicability to indoor HRI settings as compared to a model-based baseline.

## III. EXPERIMENTAL SETUP

We conducted our experiments in an open space measuring approximately 20 ft  $\times$  20 ft. Obstacles visible in Fig. 1 were outside the boundaries of the experimental volume. Cones marked the pedestrian start and goal positions. The experiments took place in a large open area in our lab, reflecting a typical environment for service robots. The participants and robot were given a simultaneous trigger to begin moving, with the participants getting an audible countdown. The Institutional Review Board of Clemson University approved the study on May 4th, 2022 under application number IRB2022-0251.

### A. Participants

Two female and seven male participants (age between 23 and 30 years old,  $M = 26.4$ ,  $SD = 2.2$ ) gave informed consent to participate in this user study. All were free of any known impediments to their walking and had normal or corrected vision, as verified by self-report. The participants were drawn from a pool of graduate students enrolled in the College of Engineering and Applied Sciences at Clemson University. The average height of the participants was  $1.77 \pm 0.10m$ , and the shoulder-to-shoulder distance was  $0.46 \pm 0.04m$ . None of the students had interacted with robots in their research, but most had been exposed to robotics somehow. The participants were not informed about the overall goal of the experiments until after the recordings had concluded to avoid any biases.

### B. Robot

The wheeled robot the participants interacted with was a TurtleBot 2 from ClearPath Robotics, shown in Fig. 1. To provide a varied dataset, we consider three local planning algorithms to steer the robot to its destination: a Linear controller that maintains a constant speed with no deviation from the straight line path to the robot’s goal, NH-TTC [12] that formulates local navigation as an optimization problem employing a time-to-collision based cost function [10], and CADRL-GAC3 [15] that learns a steering policy for the robot using reinforcement learning. We chose NH-TTC and CADRL as representative geometric and machine-learning approaches



Fig. 2. Graphical representation of the four scenarios used in the analysis for  $Q_1$ , from right to left they are *Perpendicular*, *Adjacent*, *Opposite*, and *Intersection*. Colored squares denote the goal locations of the corresponding agents (humans or robot).

for collision-free local steering, respectively. Both approaches are reactive, accounting for collisions with nearby neighbors in an anticipatory manner as opposed to Linear, which is a non-reactive approach. During our experiments, all planning nodes were run on a central server and a velocity command was relayed to the robot, ensuring no delayed robot responses. In all trials, we set the maximum robot speed at 0.5m/s. The participants were not informed about the possibility of different robot controllers.

### C. Interaction Scenes

We define an interaction scene as a combination of start and goal positions for participants and the robot. Figure 2 shows four of the seven different scenes considered in our experiments. The three scenes not displayed are *2v1*, *Overtake*, and *Head-to-Head* (see appendix for detailed descriptions). For each scene, we consider a No Robot baseline and three robot controller cases (Linear, NH-TTC, and CADRL), resulting in four different robot configurations. We define a scenario as a combination of a scene, a choice in robot configuration, and the specific order of the participants. To collect a wide array of interactions, we systematically permuted the order of the participants and the type of the robot controller to ensure that we had a No Robot control scenario for each considered participants' order. In total, we recorded 139 different scenarios. We refer to the appendix for information about the different trajectories recorded for each agent.

### D. Motion Tracking System

All trials were recorded using a tracking system based on the HTC Vive Virtual Reality system (see Fig. 1). Each participant was given a baseball cap to wear that was modified to mount an HTC Vive Tracker, allowing data collection without the use of Vive's head-mounted display. The robot was tracked with an HTC Vive Controller attached to the top shelf of the Turlebot via a custom-made bracket. The Vive System interfaced directly with a Robot Operating System (ROS) node, and each device's position was reported at 60Hz. The robot's and humans' data were obtained via the use of two HTC Lighthouses positioned on either side of the recording area. The accuracy of this system was measured at the sub-centimeter level over a distance of several meters. To reduce oscillations and remove noise, the recorded robot's

and humans' trajectories were resampled at 60Hz, and a Butterworth lowpass filter (2nd order, 0.5Hz cutoff frequency) was applied to the positions. The velocity was estimated from the displacement in the smoothed positions.

## IV. $Q_1$ : ANALYSIS OF ROBOTIC CONTROLLERS

As new local planning approaches for mobile robot navigation are being introduced, it is paramount to be able to assess the performance of such approaches. However, the majority of existing solutions are not evaluated in physical settings. In addition, the evaluation metrics used are often robot-centric rather than human-centric. While robot-centric metrics are appropriate in homogeneous environments, in shared environments, the robots should aim to maximize human safety and efficiency even at the cost of their own efficiency. To mitigate these shortcomings, we consider several human-centric metrics to evaluate the robot controllers in comparison to the cases where no robot was present. We limit our analysis to the scenes shown in Fig. 2. These scenes have sufficient samples to run statistical analysis and involve complex interactions containing all three participants in the environment and/or human-robot interactions at different angles. We hypothesize that, due to their reactive nature, state-of-the-art controllers like NH-TTC and CADRL shouldn't impact the humans' safety and efficiency and will outperform the Linear controller that doesn't react to its neighbors.

### A. Metrics

We consider three *efficiency* metrics and a *safety* metric to determine the impact each robot controller has on the participants. These metrics are calculated from the participant's perspective, rewarding human-centered behavior. Formally, given a scenario, let  $A$  denote its set of agents that include the set of human participants  $H$  and possibly a robot  $R$ . Each human participant  $H_i$  has a start position  $S_i$ , a goal position  $G_i$ , and a radius  $r_i$  determined by the shoulder-shoulder distance. Each participant also has an array of valid time steps  $T$  and, for each  $t \in T$ , the position, and velocity of the participant are denoted by  $\mathbf{p}_i^t$  and  $\mathbf{v}_i^t$ , respectively. The robot parameters are defined similarly. We define the following metrics on the human agents of the given scenario:

1) *Speed*: The speed of each human agent is calculated as the median of the L2 norm for each recorded velocity along the agent's trajectory.

TABLE I  
MEAN AND STANDARD DEVIATION FOR METRICS GROUPED BY SCENE AND CONTROLLER. SIGNIFICANT DIFFERENCES WITH RESPECT TO THE NO ROBOT CASE ARE HIGHLIGHTED IN RED ( $p < 0.05$ ). ARROWS INDICATE IF A HIGHER OR LOWER VALUE IS BETTER.

Scene	Controller	Speed (m/s) $\uparrow$	Travel Time (s) $\downarrow$	Path Linearity (m) $\downarrow$
Perpendicular	Linear	0.872 $\pm$ 0.384	12.121 $\pm$ 2.213	37.737 $\pm$ 14.259
	CADRL	1.114 $\pm$ 0.094	10.868 $\pm$ 1.207	31.219 $\pm$ 16.689
	NHTTC	1.085 $\pm$ 0.178	10.974 $\pm$ 1.69	32.579 $\pm$ 16.264
Adjacent	Linear	1.082 $\pm$ 0.156	11.417 $\pm$ 1.529	38.358 $\pm$ 29.524
	CADRL	1.064 $\pm$ 0.169	11.229 $\pm$ 1.697	33.946 $\pm$ 22.505
	NHTTC	0.942 $\pm$ 0.312	11.786 $\pm$ 1.307	35.605 $\pm$ 26.534
Opposite	Linear	1.053 $\pm$ 0.073	11.383 $\pm$ 0.875	38.885 $\pm$ 29.95
	CADRL	0.993 $\pm$ 0.171	12.252 $\pm$ 1.252	38.108 $\pm$ 27.28
	NHTTC	1.012 $\pm$ 0.117	11.884 $\pm$ 1.2	34.319 $\pm$ 28.685
Intersection	Linear	1.079 $\pm$ 0.148	10.808 $\pm$ 1.756	45.927 $\pm$ 32.669
	CADRL	1.038 $\pm$ 0.094	11.1 $\pm$ 0.922	39.958 $\pm$ 22.766
	NHTTC	0.999 $\pm$ 0.159	11.648 $\pm$ 1.621	47.102 $\pm$ 29.406

2) *Travel Time*: The total time a human agent spent traveling between the start and goal positions.

3) *Path Linearity*: The path linearity of each human agent is the sum of the absolute deviations from the straight line path from the agent’s start to the goal:

$$\sum_{t \in T} \left| \frac{\|(G_i - S_i) \times (S_i - \mathbf{p}_i^t)\|}{\|G_i - S_i\|} \right|. \quad (1)$$

The intention of this metric is not to promote straight paths but rather to ensure that the robot doesn’t impact the shape of the participant’s path too drastically.

4) *Safety*: Let  $\tau$  denote the time that it takes for the disks of two agents to collide assuming they both maintain their current velocities. Given that humans have a finite reaction time of 200-400ms and an interaction time horizon of 2-4s [10], [34], we consider any predicted collision with a  $\tau$ -value below 1.5s as potentially dangerous. The safety of each human agent is then defined as the ratio of the safe frames to all recorded trajectory frames:

$$\frac{|\{\tau(H_i^t, A_j^t) > 1.5, \forall t \in T, \forall j \neq i \in A\}|}{|T|}, \quad (2)$$

where  $A_j$  denotes either another human participant or the robot, and  $\tau(H_i, A_j)$  is a function of the relative velocity, relative displacement, and radii of the two interacting agents.

## B. Statistics

To evaluate the effect that the robot has on the participants in each of the four scenes, one-way analysis of variance was performed on each of the proposed measures using the robot type (No Robot, Linear, NH-TTC, CADRL) as independent variable. To guarantee valid comparisons, we performed a Welch ANOVA whenever the assumption of equal variance was violated and the Kruskal-Wallis nonparametric alternative to the classic ANOVA when the normality assumption did not hold [35]. To further investigate the interaction effects and determine whether introducing a robot with a specific type of controller (Linear, NH-TTC, CADRL) had a significant impact on the participants, pairwise post-hoc comparisons

were performed for each scene-metric combination between each controller and the No Robot case using the latter as the control group. These were done using Dunn’s test after nonparametric ANOVAs, and Dunnett’s and Dunnett’s T3 tests after classic and Welch ANOVAs, respectively [35].

## C. Results

The mean and standard deviation for the efficiency metrics along with the pairwise significance information of the related post-hoc tests are shown in Table I. We refer to Fig. 3 for corresponding results pertaining to the safety metric and to the appendix for the No Robot statistics.

1) *Speed*: Our results indicate a significant interaction effect for speed in all but the *Adjacent* scene. By comparing the No Robot to the robot controller cases, we observe that the participant’s speed in the *Perpendicular* scenarios is significantly reduced only when a Linear controller is employed ( $p < 0.05$ ). In contrast, in the *Intersection* scenarios, the two reactive controllers (CADRL, NH-TTC) lead to a significant decrease in speed ( $p$ -values  $< 0.05$ ) as opposed to the Linear controlled robot that does not impede the speed of the participants ( $p = 0.23$ ). Finally, in *Opposite*, a significant difference is observed between the No Robot and the robot cases for each of the three controllers ( $p < 0.01$  for NHTTC,  $p < 0.05$  for Linear and CADRL).

2) *Travel Time*: Overall, there is a significant interaction effect for travel time in all scenes. Regarding the 3-participants scenarios, in the *Opposite*, humans needed significantly more time to reach their goals regardless of the type of controller employed ( $p$ -values  $< 0.01$ ), while in *Perpendicular*, only the linear controller leads to an increase in travel time ( $p < 0.05$ ) and only NH-TTC in the *Adjacent* ( $p < 0.01$ ). In the *Intersection*, a significant difference between the No Robot and robot cases is observed only when humans interact with a reactive robot ( $p < 0.01$ ).

3) *Path Linearity*: In terms of path linearity, no interaction effect was observed in the *Adjacent* and *Opposite* scenarios. As shown in Table I, the path linearity is significantly different from the No Robot case when humans interact with a Linear controlled robot in the *Perpendicular* scenarios ( $p < 0.01$ ).



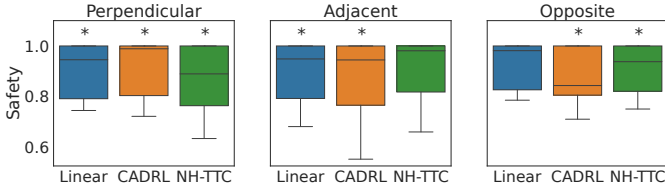


Fig. 3. Safety of human participants in the *Perpendicular*, *Adjacent*, and *Opposite* (see Eq. 2). The *Intersection* scene is not included as there are no unsafe samples. \* indicates a statistically significant deviation from the No Robot samples ( $p \leq 0.05$ ) that have an average safety of  $0.992 \pm 0.024$ .

In *Intersection*, only the NH-TTC controller significantly increases path linearity ( $p < 0.05$ ).

4) *Safety*: A significant interaction effect for safety was observed in all scenes besides the *Intersection*. In *Intersection*, no statistical comparisons were performed given the lack of variance and large mean indicating minimal unsafe frames ( $M = 0.999$  and  $SD = 0.006$ ). Figure 3 reports the corresponding statistics for the robot controllers in the other three scenes and their pairwise comparisons to the No Robot case. In *Perpendicular*, the human safety is reduced when the robot is present independent of the controller type ( $p$ -values  $< 0.05$ ). In *Adjacent*, CADRL and Linear lead to a decrease in safety ( $p$ -values  $< 0.01$ ), and the same applies to the reactive CADRL and NH-TTC controllers in the *Opposite* scenarios ( $p < 0.01$  and  $p < 0.05$ , respectively).

#### D. Discussion

Overall, when focusing on the efficiency performance per scene, the two reactive controllers are the best choice for *Perpendicular*, either Linear or CADRL for *Adjacent*, and only Linear for *Intersection*. In the *Opposite* all three controllers are equally inefficient. Similarly, in terms of the participants' safety, no controller is universally better, with NH-TTC leading to safe navigation in the *Adjacent* scenes and Linear in *Opposite*, while all controllers result in safe and unsafe interactions in *Intersection*, and *Perpendicular* scenarios, respectively. In Fig. 4, we plot the distribution of the minimal predicted distance between human-robot pairs for the three controllers assuming that the agents maintain their current velocities [34]. As can be seen, the three curves collapse onto each other highlighting the similar safety performance that all three controllers exhibit. It is clear from the above observations that, as opposed to our hypothesis before the experiments took place, reactive controllers can impede the safety and efficiency of humans and do not necessarily outperform the non-reactive Linear controller. In retrospect, this can be explained by the *duality* of the HRI problem. In HRI settings, the actions of a robot affect the behavior of the humans as much as the actions of the humans affect the behavior of the robot [36], [37]. So, when an NH-TTC or CADRL Turtlebot interacts with humans, it tries to predict what the humans will do and react accordingly, sharing the collision avoidance effort. However, such intelligent, anticipatory behavior can sometimes confuse humans and negatively influence their efficiency and safety as they try to guess the robot's behavior. In contrast, when interacting with a Turtlebot that follows a straight path, the

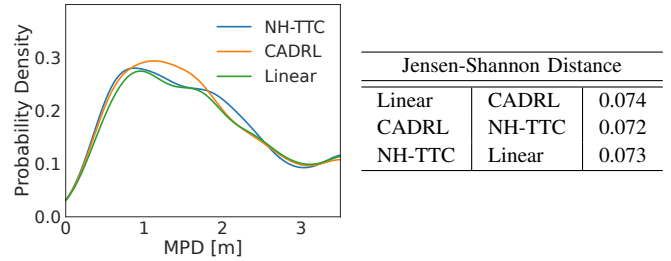


Fig. 4. (left) Distribution of the minimal predicted distance (MPD) between a human participant and the Turtlebot clustered by the type of the robot controller employed. The corresponding plots were obtained by considering the center-to-center MPD values of all distinct human-robot interaction pairs. (right) The Jensen-Shannon distance between the MPD distributions.

humans realize that the robot does not react to them and can quickly make minor adjustments to their trajectories way in advance to resolve collisions efficiently. We note that this may not be true when humans interact in more complex settings where their goals are not in direct sight. However, in our indoor settings, our analysis highlights the need for robot navigation methods that put human safety and efficiency at the forefront along with the importance of evaluating such methods from a human-centric perspective.

## V. $Q_2$ : HUMAN TRAJECTORY PREDICTION

In recent years, with the rise of deep learning techniques, many trajectory prediction approaches have shown impressive results on crowd and vehicle datasets, attributed in part to successfully reasoning about agent-agent and agent-environment interactions [33]. While such approaches can find applications to social robot navigation and facilitate more accurate human trajectory prediction, many have not tested against human-robot-interaction scenarios [2]. To address this issue, we analyze the performance of representative model-free and model-based approaches for human trajectory prediction on our Zucker dataset. Given the local nature of indoor interaction settings, we postulate that simple, linear prediction models can exhibit SOTA results.

### A. Models and Metrics

Given a local  $T$ -frame observation of a human participant's trajectory history, we aim to estimate the participant's position over the next  $H$ -frames. A straightforward prediction approach is a constant velocity model (CVM), where the future positions of an agent are inferred from its last position and velocity, assuming a linear extrapolation. In benchmarks commonly used for human trajectory prediction, such as ETH [27], UCY [38], and SDD [39], it has been shown that CVM-based approaches can rival even state-of-the-art neural network approaches [40]. As such, we use CVM as a baseline and compare its performance to two SOTA approaches for model-free trajectory prediction, Trajectron++ [32] and SocialVAE [31]. Trajectron++ employs a conditional variational autoencoder (VAE) architecture where the prior is modeled as a mixture of Gaussians. SocialVAE leverages an RNN-based timewise VAE and an attention mechanism that captures the social influence from the neighboring agents.

TABLE II  
ADE/FDE PERFORMANCE OF CVM, TRAJECTRON++, AND SOCIALVAE  
IN ZUCKER SCENES GROUPED BY DIFFERENT ROBOT CONTROLLERS.

Method	CADRL	NH-TTC	Linear	Average
CVM	0.21 / 0.42	0.19 / 0.38	0.20 / 0.41	0.20 / 0.40
Trajectron++	0.17 / 0.33	0.16 / 0.32	0.14 / 0.28	0.16 / 0.31
SocialVAE	0.16 / 0.32	0.15 / 0.29	0.15 / 0.30	0.15 / 0.30

Given the length of the recorded participants’ trajectories, we use  $T = 5$  frames as the observation window and  $H = 8$  frames as the prediction horizon. To perform predictions, we resampled the Zucker data at 2.5FPS, which led to an observation window of 2s and a prediction horizon of 3.2s. While the publicly available Trajectron++ and SocialVAE code offers many pre-trained models, we had to retrain them to fit the new horizons. To do so, we use the Univ dataset from the UCY benchmark [38]. Following the literature, we use the Average Displacement Error (ADE) and the Final Displacement Error (FDE) to evaluate the performance of the two models and the CVM baseline. Given the multimodal predictions of Trajectron++ and SocialVAE, we report the minimum ADE/FDE over the top-5 predictions.

### B. Results

In Table II, we report the performance of CVM, Trajectron++, and SocialVAE on the human-robot interaction cases from our Zucker dataset, grouped by the three robot controller types. As can be seen, the model-free approaches outperform the CVM baseline, with the ADE/FDE values being similar across the different robot controllers. SocialVAE, as a more recent approach, achieves better overall ADE/FDE performance. To better understand these results, we also compute the performance of the considered trajectory prediction approaches on the Zara01, Zara02, and Univ crowd datasets from the UCY benchmark. In Fig. 5, we report the performance improvement of Trajectron++ and SocialVAE over CVM for both the UCY and Zucker datasets. Similar to Zucker, the model-free approaches outperform CVM in UCY. However, the performance improvement is much more significant in these datasets, with Trajectron++ and SocialVAE achieving on average a 27% and 47% FDE improvement, respectively, as opposed to a 23% and 26% improvement in Zucker. We refer to the supplementary material for detailed results.

### C. Discussion

The performance of the CVM baseline can provide a quick way to assess the interaction complexity in the scene [40]. Small ADE/FDE values typically denote that humans exhibit mostly linear interactions, with the past trajectory of a tracked human being the main feature for predicting its future. Given the CVM performance in our dataset, one could argue that humans undergo less complex social interactions in Zucker than in the UCY datasets. As such, employing a linear model to track the trajectories of humans in similar HRI indoor settings is a strong baseline, especially as more complex methods might introduce unnecessary computational overhead in an

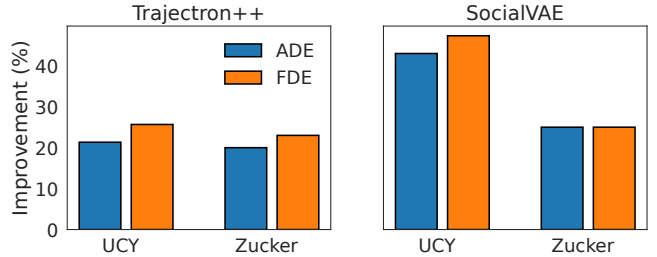


Fig. 5. Percentage improvement over the Constant Velocity Model for Trajectron++ and SocialVAE on the UCY and Zucker datasets. The Zucker results are obtained using all three robot steering controllers.

already strained real-time setting. On the other hand, learning-based approaches such as Trajectron++ and SocialVAE attain better overall prediction performance and are more powerful, providing more insight. Indeed, recent works have successfully exploited model-free prediction approaches to inform more human-aware robot control in indoor settings [41]. Finally, as we note in Fig. 5, the performance improvement over CVM for SocialVAE is much lower in our Zucker dataset than in the human-only datasets commonly used in trajectory prediction benchmarks. This indicates that there is potential room to improve the performance of human trajectory prediction methods in indoor HRI settings by training models with more representative datasets, devising new models, and/or refining trained models both in online and lifelong manners [42].

## VI. $Q_3$ : HUMAN-ROBOT INTERACTION LAW

In [10], it was shown that the interaction law between pairs of humans in a crowd follows an inverse power-law relationship with their projected time to collision and is therefore anticipatory depending not just on the current state of the environment but also on the expected future states. While this simple law consistently holds across different conditions and settings, it was derived from analyzing various human-only datasets, including the UCY data. Here, we are interested in answering whether the same anticipatory law applies when humans interact with robots in indoor, heterogeneous environments like the ones considered in our user study. We hypothesize that humans will be more cautious and try to avoid collisions with the Turtlebots as early as possible compared to the human-human interaction behavior observed in crowd-only scenes.

### A. Methodology

Following [10], we focus on the time to collision metric,  $\tau$ , and employ a probabilistic analysis approach to study pairwise interactions in isolation from all other factors that can influence the behavior of agents. To do so, we compare the frequency of  $\tau$ -values between human-robot pairs that appear in a recorded scene at the same time to the frequency of  $\tau$ -values for random, non-interacting pairs. The resulting normalized frequency estimates the pair distribution function,  $g(\tau)$ , that highlights statistically suppressed interactions. Such a function can be converted to a “social interaction energy”,  $E$ , assuming a Boltzmann-like relation between  $g$  and  $E$ :  $E(\tau) \propto \log(1/g(\tau))$ . Thus, the energy vanishes when  $g(\tau) = 1$  and drastically increases for small  $g(\tau)$  values.

## B. Results

Figure 6 shows the pair distribution function  $g(\tau)$  from the Zucker dataset. The reported plots were obtained by considering  $\tau$ -values for human-robot-only pairs. Overall, the NH-TTC and CADRL curves show very similar behavior, allowing us to combine them and estimate the normalized distribution of the  $\tau$ -values between the human participants and predictive robot controllers. In Fig. 6, we show the interaction energy  $E(\tau)$  derived from  $g(\tau)$ . To gain a better understanding of these results, we also depict the interaction energy graph from [10] obtained by analyzing pedestrian interactions in the UCY crowd scenes. As can be seen, in both our HRI scenes and the crowd interaction scenes, humans don't care about collisions that will take place in the far future, with  $E(\tau) \approx 0$  for  $\tau > 1.5$ s. Furthermore, the energy increases as  $\tau$  decreases, highlighting humans' anticipatory nature whether they interact with other humans or robots. However, it is highly unlikely for two pedestrians in a crowd to arrive at a situation where a collision is imminent, as the interaction energy rises to infinity when  $\tau < 0.3$  s. In contrast, in the Zucker dataset, it is likely to encounter human-robot pairs that have imminent collisions, as  $g(\tau) \approx 0.25$  for  $\tau < 0.3$ s, resulting in the interaction energy fluctuating around a constant value for such  $\tau$ 's.

## C. Discussion

Our results show that the human-robot interaction law differs somewhat from the human-human interaction law. Overall, humans anticipate collisions when interacting with other agents (humans or Turtlebots), with the energy increasing with decreasing time-to-collision values. However, when faced with an imminent collision, and in contrast to what we expected before the experiments, the interaction energy between a human and a Turtlebot is finite as opposed to human-human interactions that exhibit infinite energy.

In hindsight, such a finding is not that surprising. Turtlebots can only cause a finite amount of social discomfort compared to other classes of agents, as they move slowly and are not intimidating. For example, we typically step over Roombas, highlighting our lack of any fear of colliding with them. Hence, humans are more willing to head toward a collision since they can resolve it quickly. We note that during our HRI experiments, no actual collisions took place, though several near collisions were observed (in Fig. 6, the positive  $g(\tau)$  value for  $\tau = 0$  is due to the binning of  $\tau$ ). We expect the observed human-robot interaction law to extend to other small indoor robots leading to the development of more accurate models of human behavior compared to the ones currently employed in robot simulators [9], [10], [25], [26]. We acknowledge, though, that such finite interaction forces may not apply to larger indoor robots such as humanoids or fast-moving transport robots deployed in fulfillment centers.

## VII. CONCLUSION

In this paper, we study how human behavior is affected by different types of robot controllers in indoor navigation settings by focusing on three key HRI questions. We conclude by drawing some overall recommendations from our study.

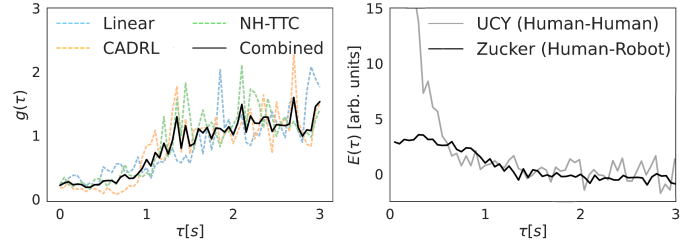


Fig. 6. (left) The pair distribution function  $g$  as a function of the projected time-to-collision value  $\tau$  between human-robot pairs. The curves are grouped based on the type of controller that the robot employs and exhibit similar behavior, allowing us to combine them. (right) The corresponding interaction energy  $E$  remains finite even for small  $\tau$ -values, as opposed to the human-human interaction energy inferred from the UCY crowd dataset (obtained from [10]). The energy curves are normalized so that  $E(1) = 1$ .

Regarding  $Q_1$ , we believe that methods for social robot navigation should be evaluated based not only on the performance of the robot but also on how well the humans in the scene perform. Our analysis shows no clear preference between non-reactive and intelligent, predictive controllers when assessing the impact they have on the efficiency and safety of humans, with a simple linear controller being in many cases better than the more intelligent ones. As such, and despite recent advancements, the community needs to invest in more *human-centered* methods for mobile indoor navigation [43], seeking to prioritize human safety and efficiency over robot performance (e.g., for tasks like vacuuming that aren't constrained by time) or maximize the joint performance of the entire social robot navigation system [2]. Along this direction, recent work has explored group-aware robot planning techniques and collaborative strategies for robot collision avoidance among others [19]–[21], [44].

Regarding  $Q_2$ , we believe that existing models for human trajectory prediction can benefit from real-world HRI datasets, like the one we provide in this paper, allowing their implementation on actual robots and informing more socially-aware control. That being said, as we show in our analysis, there is still a long way to achieve SOTA prediction performance, given that the uncertainty in human decision-making can be exacerbated in robot interaction settings. In that regard, we need models that can successfully reason not only human-human interactions but also human-robot interactions [33]. In learning-based approaches, for example, specialized observation encoding modules can be tasked with different types of interactions. Similarly, continual learning approaches can help improve the predictive power of existing human trajectory prediction models in settings where human behavior adapts to the robot continuously [42].

Regarding  $Q_3$ , we believe that existing robot simulators could benefit from more accurate pedestrian dynamics models. In existing simulators commonly used to train social robot navigation algorithms (e.g., [15], [18]) and in benchmarking tools (e.g., [24], [25]), human behavior is typically modelled with distance-based potentials [26] or anticipatory ones based on the notion of time to collision [9], [10]. However, our analysis shows that humans interact with small differential drives differently than they would with humans when collisions are imminent, suggesting a combination of the two potentials. Basically, humans anticipate and try to avert collisions with

the robot but such collisions impose a finite level of discomfort. Such human-robot interaction laws could be combined with existing human-human interaction models to create more realistic pedestrian simulations that can facilitate the training and evaluation of robot navigation methods and inform more human-centered robot control.

## REFERENCES

- [1] L. Eliot, “Self-driving cars and Asimov’s three laws about robots,” January 2021, [Online].
- [2] C. Mavrogiannis, F. Baldini, A. Wang, D. Zhao, P. Trautman, A. Steinfeld, and J. Oh, “Core challenges of social robot navigation: A survey,” *ACM Trans. Hum.-Robot. Interact.*, vol. 12, no. 3, pp. 1–39, 2023.
- [3] Z. Yan, S. Schreiberhuber, G. Halmetschlager, T. Duckett, M. Vincze, and N. Bellotto, “Robot perception of static and dynamic objects with an autonomous floor scrubber,” *Intell. Serv. Robot.*, vol. 13, no. 3, pp. 403–417, 2020.
- [4] R. Martin-Martin, M. Patel, H. Rezaatofghi, A. Sheno, J. Gwak, E. Frankel, A. Sadeghian, and S. Savarese, “Jrdb: A dataset and benchmark of egocentric robot visual perception of humans in built environments,” *IEEE Trans. Pattern Anal. Mach. Intell.*, 2021.
- [5] H. Karnan, A. Nair, X. Xiao, G. Warnell, S. Pirk, A. Toshev, J. Hart, J. Biswas, and P. Stone, “Socially compliant navigation dataset (scand): A large-scale dataset of demonstrations for social navigation,” *IEEE Robot. Autom. Lett.*, vol. 7, no. 4, pp. 11 807–11 814, 2022.
- [6] A. Rudenko, T. P. Kucner, C. S. Swaminathan, R. T. Chadalavada, K. O. Arras, and A. J. Lilienthal, “Thör: Human-robot navigation data collection and accurate motion trajectories dataset,” *IEEE Robot. Autom. Lett.*, vol. 5, no. 2, pp. 676–682, 2020.
- [7] B. Zhang, J. Amirian, H. Eberle, J. Pettré, C. Holloway, and T. Carlson, “From hri to cri: Crowd robot interaction—understanding the effect of robots on crowd motion,” *Int. J. Soc. Robot.*, vol. 14, no. 3, pp. 631–643, 2022.
- [8] Z. Chen, C. Jiang, and Y. Guo, “Pedestrian-robot interaction experiments in an exit corridor,” in *IEEE Int. Conf. Ubiquitous Robot.*, 2018, pp. 29–34.
- [9] J. van den Berg, S. J. Guy, M. Lin, and D. Manocha, “Reciprocal n-body collision avoidance,” in *Robot. Res.*, 2011, pp. 3–19.
- [10] I. Karamouzas, B. Skinner, and S. J. Guy, “Universal power law governing pedestrian interactions,” *Phys. Rev. Lett.*, vol. 113, no. 23, p. 238701, 2014.
- [11] Y. Luo, P. Cai, A. Bera, D. Hsu, W. S. Lee, and D. Manocha, “Porca: Modeling and planning for autonomous driving among many pedestrians,” *IEEE Robot. Autom. Lett.*, vol. 3, no. 4, pp. 3418–3425, 2018.
- [12] B. Davis, I. Karamouzas, and S. J. Guy, “NH-TTC: A gradient-based framework for generalized anticipatory collision avoidance,” *Robot. Sci. Syst.*, 2020.
- [13] T. Fan, P. Long, W. Liu, and J. Pan, “Distributed multi-robot collision avoidance via deep reinforcement learning for navigation in complex scenarios,” *Int. J. Robot. Res.*, vol. 39, no. 7, pp. 856–892, 2020.
- [14] A. J. Sathyamoorthy, J. Liang, U. Patel, T. Guan, R. Chandra, and D. Manocha, “Densecavoid: Real-time navigation in dense crowds using anticipatory behaviors,” in *IEEE Int. Conf. Robot. Autom.*, 2020, pp. 11 345–11 352.
- [15] M. Everett, Y. F. Chen, and J. P. How, “Collision avoidance in pedestrian-rich environments with deep reinforcement learning,” *IEEE Access*, vol. 9, pp. 10 357–10 377, 2021.
- [16] P. Trautman, J. Ma, R. M. Murray, and A. Krause, “Robot navigation in dense human crowds: Statistical models and experimental studies of human–robot cooperation,” *Int. J. Robot. Res.*, vol. 34, no. 3, pp. 335–356, 2015.
- [17] Y. F. Chen, M. Everett, M. Liu, and J. P. How, “Socially aware motion planning with deep reinforcement learning,” in *IEEE Int. Conf. Intell. Robots Syst.*, 2017, pp. 1343–1350.
- [18] C. Chen, Y. Liu, S. Kreiss, and A. Alahi, “Crowd-robot interaction: Crowd-aware robot navigation with attention-based deep reinforcement learning,” in *IEEE Int. Conf. Robot. Autom.*, 2019, pp. 6015–6022.
- [19] C. Mavrogiannis, K. Balasubramanian, S. Poddar, A. Gandra, and S. S. Srinivasa, “Winding through: Crowd navigation via topological invariance,” *IEEE Robot. Autom. Lett.*, vol. 8, no. 1, pp. 121–128, 2022.
- [20] K. Katyal, Y. Gao, J. Markowitz, S. Pohland, C. Rivera, I.-J. Wang, and C.-M. Huang, “Learning a group-aware policy for robot navigation,” in *IEEE Int. Conf. Intell. Robots Syst.*, 2022, pp. 11 328–11 335.
- [21] D. Gonon and A. Billard, “Inverse reinforcement learning of pedestrian–robot coordination,” *IEEE Robot. Autom. Lett.*, 2023.
- [22] P. Bevilacqua, M. Frego, D. Fontanelli, and L. Palopoli, “Reactive planning for assistive robots,” *IEEE Robot. Autom. Lett.*, vol. 3, no. 2, pp. 1276–1283, 2018.
- [23] A. Biswas, A. Wang, G. Silvera, A. Steinfeld, and H. Admoni, “Socnavbench: A grounded simulation testing framework for evaluating social navigation,” *ACM Trans. Hum.-Robot Interact.*, vol. 11, no. 3, pp. 1–24, 2022.
- [24] N. Tsoi, A. Xiang, P. Yu, S. S. Sohn, G. Schwartz, S. Ramesh, M. Hussein, A. W. Gupta, M. Kapadia, and M. Vázquez, “Sean 2.0: Formalizing and generating social situations for robot navigation,” *IEEE Robot. Autom. Lett.*, vol. 7, no. 4, pp. 11 047–11 054, 2022.
- [25] L. Kästner, T. Bhuiyan, T. A. Le, E. Treis, F. Cox, B. Meinardus, J. Kmiecik, R. Carstens, D. Pichel, B. Fatloun *et al.*, “Arena-Bench: A benchmarking suite for obstacle avoidance approaches in highly dynamic environments,” *IEEE Robot. Autom. Lett.*, vol. 7, no. 4, pp. 9477–9484, 2022.
- [26] D. Helbing, I. Farkas, and T. Vicsek, “Simulating dynamical features of escape panic,” *Nature*, vol. 407, no. 6803, pp. 487–490, 2000.
- [27] S. Pellegrini, A. Ess, K. Schindler, and L. Van Gool, “You’ll never walk alone: Modeling social behavior for multi-target tracking,” in *IEEE Int. Conf. Comput. Vis.*, 2009, pp. 261–268.
- [28] A. Alahi, K. Goel, V. Ramanathan, A. Robicquet, L. Fei-Fei, and S. Savarese, “Social LSTM: Human trajectory prediction in crowded spaces,” in *IEEE Conf. Comput. Vis. Patt. Recognit.*, 2016, pp. 961–971.
- [29] A. Vemula, K. Muelling, and J. Oh, “Social attention: Modeling attention in human crowds,” in *IEEE Int. Conf. Robot. Autom.*, 2018, pp. 4601–4607.
- [30] A. Gupta, J. Johnson, L. Fei-Fei, S. Savarese, and A. Alahi, “Social GAN: Socially acceptable trajectories with generative adversarial networks,” in *IEEE Conf. Comput. Vis. Patt. Recognit.*, 2018, pp. 2255–2264.
- [31] P. Xu, J.-B. Hayet, and I. Karamouzas, “Socialvae: Human trajectory prediction using timewise latents,” *European Conf. Comput. Vis.*, pp. 511–528, 2022.
- [32] T. Salzmann, B. Ivanovic, P. Chakravarty, and M. Pavone, “Trajectron++: Dynamically-feasible trajectory forecasting with heterogeneous data,” in *European Conf. Comput. Vis.*, 2020, pp. 683–700.
- [33] A. Rudenko, L. Palmieri, M. Herman, K. M. Kitani, D. M. Gavrila, and K. O. Arras, “Human motion trajectory prediction: a survey,” *Int. J. Robot. Res.*, vol. 39, no. 8, pp. 895–935, 2020.
- [34] A.-H. Olivier, A. Marin, A. Créteil, and J. Pettré, “Minimal predicted distance: A common metric for collision avoidance during pairwise interactions between walkers,” *Gait & Posture*, vol. 36, no. 3, pp. 399–404, 2012.
- [35] J. Hsu, *Multiple comparisons: theory and methods*. CRC Press, 1996.
- [36] D. Sadigh, S. S. Sastry, S. A. Seshia, and A. Dragan, “Information gathering actions over human internal state,” in *IEEE Int. Conf. Intell.*, 2016, pp. 66–73.
- [37] P. Trautman and A. Krause, “Unfreezing the robot: Navigation in dense, interacting crowds,” in *IEEE Int. Conf. Intell. Robots Syst.*, 2010, pp. 797–803.
- [38] A. Lerner, Y. Chrysanthou, and D. Lischinski, “Crowds by example,” *Comput. Graph. Forum*, vol. 26, no. 3, pp. 655–664, 2007.
- [39] A. Robicquet, A. Sadeghian, A. Alahi, and S. Savarese, “Learning social etiquette: Human trajectory prediction in crowded scenes,” in *European Conf. Comput. Vis.*, vol. 2, 2020.
- [40] C. Schöller, V. Aravantinos, F. Lay, and A. Knoll, “What the constant velocity model can teach us about pedestrian motion prediction,” *IEEE Robot. Autom. Lett.*, vol. 5, no. 2, pp. 1696–1703, 2020.
- [41] S. Liu, P. Chang, Z. Huang, N. Chakraborty, K. Hong, W. Liang, D. Livingston McPherson, J. Geng, and K. Driggs-Campbell, “Intention aware robot crowd navigation with attention-based interaction graph,” in *IEEE Int. Conf. Robot. Autom.*, 2023.
- [42] L. Knoedler, C. Salmi, H. Zhu, B. Brito, and J. Alonso-Mora, “Improving pedestrian prediction models with self-supervised continual learning,” *IEEE Robot. Autom. Lett.*, vol. 7, no. 2, pp. 4781–4788, 2022.
- [43] C. Vassallo, A.-H. Olivier, P. Souères, A. Créteil, O. Stasse, and J. Pettré, “How do walkers behave when crossing the way of a mobile robot that replicates human interaction rules?” *Gait & posture*, vol. 60, pp. 188–193, 2018.
- [44] M. Sun, F. Baldini, P. Trautman, and T. Murphey, “Move beyond trajectories: Distribution space coupling for crowd navigation,” in *Robot. Sci. Syst.*, 2021.



# A Study in Zucker: Insights on Human-Robot Interactions

## Supplementary Material

Alex Day and Ioannis Karamouzas

TABLE S1  
PARTICIPANT INFORMATION

Index	# Trajectories	Height (m)	Radius (m)	Gender
-1 (Robot)	100	0.41	0.18	N/A
3	56	1.91	0.23	Female
4	56	1.75	0.24	Male
5	50	1.63	0.2	Male
6	57	1.63	0.2	Female
7	51	1.88	0.24	Male
8	51	1.73	0.22	Male

### I. EXPERIMENTAL SETUP

#### A. Zucker Dataset Information

Table S1 describes the number of trajectories and information for all participants in our HRI study.

In Table S2, we also show how the resulting Zucker dataset compares to other similar datasets in terms of experimental trials, overall recording time, robot controllers, and type of interactions.

#### B. Interaction Scenes

The following four scenes were used in  $Q_1$ ,  $Q_2$ , and  $Q_3$  (see Figure 2 in the main text):

- 1) **Perpendicular:** Three pedestrians start in a line-abreast formation and have to walk to their goals directly ahead of them while crossing paths perpendicularly with a robot.
- 2) **Adjacent:** Three pedestrians start in a line-abreast formation and have to walk to their goals directly ahead of them while crossing paths with a robot at an acute angle.
- 3) **Opposite:** Three pedestrians start in a line-abreast formation and have to walk to their goals directly ahead of them while crossing paths with a robot at an obtuse angle.
- 4) **Intersection:** Two pedestrians stand opposite each other with the goal of swapping their positions. A small offset is added to avoid symmetrical patterns. The robot and its goal are placed on a line orthogonal to the pedestrian's trajectories.

The following scenes were used only in  $Q_2$  and  $Q_3$  (see Fig. S1):

- 1) **Overtake:** The robot starts ahead of the pedestrian and their goals lie on the same line.
- 2) **Head-to-Head:** A robot and a pedestrian cross paths while approaching from opposite sides of the environment. The robot's goal is behind the pedestrian's starting position and vice versa.

TABLE S2  
COMPARISON OF RELATED HUMAN-ROBOT INTERACTION DATASETS

Name	# Trials	Time (hh:mm)	Type
THÖR	13	00:60	Structured
JRDB	54	01:04	Unstructured
FLOBOT	6	00:27	Unstructured
SCAND	138	08:42	Unstructured
<b>Zucker</b>	141	00:27	Structured

- 3) **2v1:** A group of two pedestrians has to swap positions with a standalone robot. The pedestrian goals lie on either side of the robot's starting position, and the robot's goal is between the pedestrians' start positions.



Fig. S1. Visualization of the three scenarios not used in the analysis for  $Q_1$ . From right to left they are *2v1*, *Head-to-Head*, and *Overtake*. Colored squares denote the goal locations of the corresponding agents (humans or robot).

## II. Q1 : ANALYSIS OF ROBOTIC CONTROLLERS

### A. No Robot Efficiency Metrics

In Table S3, we report the efficiency metrics for the No Robot scenarios used in  $Q_1$ . The corresponding *Perpendicular*, *Opposite*, and *Adjacent* scenarios are all collapsed into the *3-Agents* scene because the start and goal locations of the pedestrians is identical in all three and no robot is present.

### B. Minimum Predicted Distance

In Fig. 4 of the main text, we report the distribution of the *minimal predicted distance* (MPD) between human-robot pairs for each of the three robot controllers. Here, we compute the MPD as the closest center-to-center distance between the

TABLE S3  
EFFICIENCY METRICS FOR THE NO ROBOT SCENARIOS. THE 3-AGENTS  
SCENE ENCOMPASSES THE *Perpendicular*, *Opposite*, AND *Adjacent*  
SCENARIOS.

Scene	Speed (m/s)	Travel Time (s)	Path Linearity (m)
3-Agents	1.134 ± 0.081	10.531 ± 0.509	21.431 ± 8.813
Intersection	1.164 ± 0.054	9.535 ± 0.646	20.29 ± 9.381

two interacting parties assuming a linear extrapolation of their current velocities. Formally, given two agents  $A_i$  and  $A_j$ , located at  $\mathbf{p}_i$  and  $\mathbf{p}_j$ , respectively, and having velocities  $\mathbf{v}_i$  and  $\mathbf{v}_j$ , the MPD is defined as in [1]:

$$\min_{t \geq 0} \|(\mathbf{x}_i - \mathbf{x}_j) + (\mathbf{v}_i - \mathbf{v}_j) t\|. \quad (\text{S1})$$

This metric allows us to quantify the actual and predicted amount of personal space humans maintain when interacting with the different types of robots. For example, if a controller has an MPD distribution with peaks inside the personal space of humans (typically between 0.76 to 1.22 m [2]), we can categorize it differently than a controller with peaks further away. As shown in the figure, all three robot controllers exhibit similar MPD distributions both qualitatively and quantitatively.

### III. Q2: HUMAN TRAJECTORY PREDICTION

Table S4 shows the results of the various trajectory prediction methods on the testing subsets of the UCY dataset [3]. Both Trajectron++ [4] and SocialVAE [5] models were trained and tested with 5 frames of history and 8 frames of prediction

to adhere to the results reported in Table III of the main text. Given the multimodal predictions of both models, we report the minimum ADE/FDE over the top-5 predictions, with SocialVAE using a Final Position Clustering technique in post-processing to help reduce sampling bias [5]. We refer to the official repositories of Trajectron++ and SocialVAE for additional details. CVM produces deterministic predictions assuming that the agents maintain their last observed velocities for 8 consecutive frames.

TABLE S4  
ADE/FDE PERFORMANCE OF CVM, TRAJECTIONS++, AND SOCIALVAE  
IN THE UCY CROWD DATASETS MEASURED IN METERS.

Method	Zara01	Zara02	Univ
CVM	0.26 / 0.55	0.22 / 0.47	0.32 / 0.68
Trajectron++	0.20 / 0.40	0.17 / 0.34	0.26 / 0.53
SocialVAE	0.17 / 0.35	0.14 / 0.28	0.13 / 0.23

### REFERENCES

- [1] A.-H. Olivier, A. Marin, A. Crétual, and J. Pettré, “Minimal predicted distance: A common metric for collision avoidance during pairwise interactions between walkers,” *Gait & Posture*, vol. 36, no. 3, pp. 399–404, 2012.
- [2] E. T. Hall, *The hidden dimension*. Anchor, 1966.
- [3] A. Lerner, Y. Chrysanthou, and D. Lischinski, “Crowds by example,” *Comput. Graph. Forum*, vol. 26, no. 3, pp. 655–664, 2007.
- [4] T. Salzmann, B. Ivanovic, P. Chakravarty, and M. Pavone, “Trajectron++: Dynamically-feasible trajectory forecasting with heterogeneous data,” in *European Conf. Comput. Vis.*, 2020, pp. 683–700.
- [5] P. Xu, J.-B. Hayet, and I. Karamouzas, “Socialvae: Human trajectory prediction using timewise latents,” *European Conf. Comput. Vis.*, pp. 511–528, 2022.